



HAL
open science

Anisotropy of the anomalous Hall effect in the altermagnet candidate Mn_5Si_3 films

Miina Leiviskä, Javier Rial, Antonín Badura, Rafael Lopes Seeger, Ismaïla Kounta, Sebastian Beckert, Dominik Kriegner, Isabelle Joumard, Eva Schmoranzarová, Jairo Sinova, et al.

► **To cite this version:**

Miina Leiviskä, Javier Rial, Antonín Badura, Rafael Lopes Seeger, Ismaïla Kounta, et al.. Anisotropy of the anomalous Hall effect in the altermagnet candidate Mn_5Si_3 films. 2024. hal-04376117

HAL Id: hal-04376117

<https://hal.science/hal-04376117>

Preprint submitted on 6 Jan 2024

HAL is a multi-disciplinary open access archive for the deposit and dissemination of scientific research documents, whether they are published or not. The documents may come from teaching and research institutions in France or abroad, or from public or private research centers.

L'archive ouverte pluridisciplinaire **HAL**, est destinée au dépôt et à la diffusion de documents scientifiques de niveau recherche, publiés ou non, émanant des établissements d'enseignement et de recherche français ou étrangers, des laboratoires publics ou privés.



Distributed under a Creative Commons Attribution 4.0 International License

Anisotropy of the anomalous Hall effect in the altermagnet candidate Mn_5Si_3 films

Miina Leiviskä,¹ Javier Rial,¹ Antonín Badura,^{2,3} Rafael Lopes Seeger,¹ Ismaïla Kounta,⁴ Sebastian Beckert,⁵ Dominik Kriegner,^{5,3} Isabelle Joumard,¹ Eva Schmoranzarová,² Jairo Sinova,⁶ Olena Gomonay,⁶ Andy Thomas,^{5,7} Sebastian T. B. Goennenwein,⁸ Helena Reichlová,⁵ Libor Šmejkal,^{6,3} Lisa Michez,⁴ Tomáš Jungwirth,³ and Vincent Baltz¹

¹*Univ. Grenoble Alpes, CNRS, CEA, Grenoble INP, IRIG-SPINTEC, F-38000 Grenoble*

²*Department of Chemical Physics and Optics, Faculty of Mathematics and Physics, Charles University, Prague, Czechia*

³*Institute of Physics, Czech Academy of Sciences, Prague, Czechia*

⁴*Aix-Marseille University, CNRS, CINaM, Marseille, France*

⁵*Institute of Solid State and Materials Physics, TU Dresden, Dresden, Germany*

⁶*Institute for Physics, Johannes Gutenberg University Mainz, Mainz, Germany*

⁷*Leibniz Institute of Solid State and Materials Science (IFW Dresden), Helmholtzstr. 20, 01069 Dresden, Germany*

⁸*Department of Physics, University of Konstanz, Konstanz, Germany*

Altermagnets are compensated magnets belonging to spin symmetry groups that allow alternating spin polarizations both in the coordinate space of the crystal and in the momentum space of the electronic structure. In these materials the anisotropic local crystal environment of the different sublattices lowers the symmetry of the system so that the opposite-spin sublattices are connected only by rotations, which results in an unconventional spin-polarized band structure in the momentum space. This low symmetry of the crystal structure is expected to be reflected in the anisotropy of the anomalous Hall effect. In this work, we study the anisotropy of the anomalous Hall effect in epitaxial thin films of Mn_5Si_3 , an altermagnetic candidate material. We first demonstrate a change in the relative Néel vector orientation when rotating the external field orientation through systematic changes in both the anomalous Hall effect and the anisotropic longitudinal magnetoresistance. We then show that the anomalous Hall effect in this material is anisotropic with the Néel vector orientation relative to the crystal structure and that this anisotropy requires high crystal quality and unlikely correlates with the magnetocrystalline anisotropy. Our results provide further systematic support to the case for considering epitaxial thin films of Mn_5Si_3 as an altermagnetic candidate material.

I. INTRODUCTION

The physical properties of magnetic materials are governed by the intrinsic symmetries of their crystal and spin structures, which are represented by symmetry groups. A good example in the realm of magnetotransport properties is the anomalous Hall effect (AHE) [1], where a longitudinal electric field \mathbf{E} generates a transversal Hall current \mathbf{j}_H that is perpendicular to the Hall vector ($\mathbf{h} = (\sigma_{zy}, \sigma_{xz}, \sigma_{yx})^T$, where σ_{ij} are the off-diagonal terms of the conductivity matrix) i.e. $\mathbf{j}_H = \mathbf{h} \times \mathbf{E}$. As \mathbf{h} is an axial vector and odd upon time-reversal (\mathcal{T}), non-vanishing AHE is only observed in systems where the symmetries allow for such a vector. In ferromagnetic materials the net magnetization is also a \mathcal{T} -odd axial vector and thus \mathbf{h} is allowed [1] while in magnetic materials with compensated order, \mathbf{h} is allowed upon sufficient lowering of the crystal symmetries [2–7]. In antiferromagnetic materials [8, 9] where the opposite-spin sublattices are connected by translation or inversion, \mathbf{h} is forbidden by symmetry, while in altermagnetic materials [10] this connecting symmetry is rotation, which allows for \mathbf{h} [11–17]. This lowered symmetry in altermagnets stems from the two sublattices being inequivalent in terms of the local crystal environment. Altermagnets are characterised by alternating spin-splitting of the energy bands [18–22] and they show various core spintronic properties such as the AHE presented above, the Nernst effect (thermal counterpart of the AHE) [23], spin-polarized current generation [24–26], as well as giant and tunnel magnetoresistances [27–29] in heterostructures.

In polycrystalline soft ferromagnets, \mathbf{h} is allowed by symmetry for any magnetization orientation. Therefore, the AHE

is proportional to the component of the magnetization that is parallel to \mathbf{h} , i.e. to $M_S \cos \theta$, where M_S is the saturation magnetization and θ is the angle between the external field and the film normal, assuming that the field is strong enough to saturate the magnetization. Exceptions to this behavior can arise in crystalline ferromagnets [30, 31] or ferromagnets with strong magnetocrystalline anisotropy, which causes a lag between the external field and the magnetization. In altermagnets, specific Néel vector (\mathbf{L}) orientations can either allow or exclude the Hall vector $\mathbf{h}(\mathbf{L})$ by symmetry [7, 11, 13] so that anisotropic AHE beyond $M_S \cos \theta$ can arise.

Anisotropic AHE beyond $M_S \cos \theta$ in compensated magnets constitutes a hallmark of altermagnetism, as has been recently demonstrated in RuO_2 [11] (intrinsic d-wave altermagnet, i.e. the electronic structure displays four lobes with alternating spin-polarization) and MnTe showing spontaneous AHE [13] (intrinsic g-wave, which acquires a d-wave character in the presence of spin-orbit coupling). Both RuO_2 and MnTe owe their altermagnetism to the presence of non-magnetic atoms that lower the symmetry of the system such that the opposite-spin sublattices are not connected by either inversion or translation [10]. The saturation of \mathbf{L} in RuO_2 and MnTe requires high fields of 68 [11, 12] and 4 T [13], respectively, so for further studies on the anisotropy of AHE in altermagnets a new material candidate where \mathbf{L} -saturation is realized at smaller fields would be ideal.

Recently, epitaxial thin films of Mn_5Si_3 have emerged as such candidate [15] as the collinear compensated phase of Mn_5Si_3 with a hexagonal unit cell and four magnetic Mn atoms on the Mn2 sites in a checkerboard arrangement of the sublattices shown in Figure 1(a) fulfills the symmetry crite-

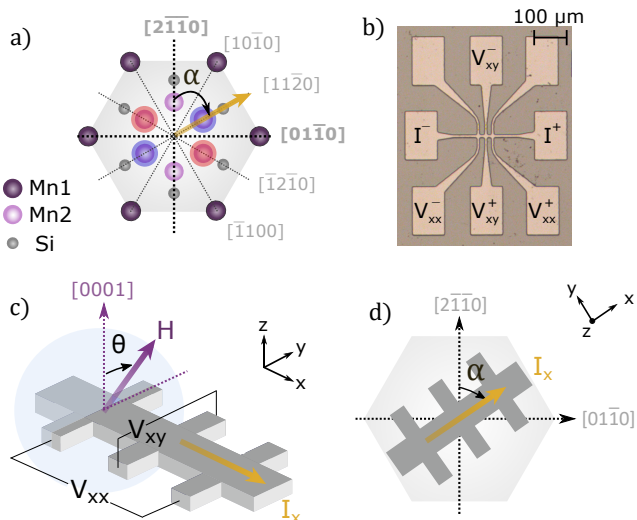


FIG. 1. (Color Online) (a) The hexagonal unit cell of epitaxial thin films of Mn_5Si_3 . The two magnetically ordered opposite-spin sublattices of Mn-atoms are highlighted in red and blue. Note, that there are two other options ('quadrupole domains') for the checkerboard distribution of the magnetic Mn atoms among the Mn2 sites. (b) Optical image of a typical Hall bar device. (c) Illustration of a Hall bar with the angle θ defining the external field H orientation relative to the film normal z , which coincides with the $[0001]$ crystal axis of Mn_5Si_3 . (d) Top view of a Hall bar showing the angle α , which refers to the orientation of the current channel I_x relative to the crystal axis $[0\bar{1}10]$. Varying α is achieved through the fabrication of a set of Hall bars oriented along several crystal directions.

ria for altermagnetism [15]. Note, that in the bulk phase of Mn_5Si_3 the hexagonal unit cell is not preserved during the magnetic ordering and the opposite-spin sublattices become connected by translation making bulk Mn_5Si_3 antiferromagnetic [32–35]. However, when grown as epitaxial thin films [16] the substrate stabilises the hexagonal unit cell of Mn_5Si_3 over the entire temperature range [15], fulfilling the symmetry requirements for making epitaxial Mn_5Si_3 a potential candidate for the altermagnetic phase with a d-wave symmetry. In good accordance with the theoretical predictions and the structural properties epitaxial Mn_5Si_3 exhibits a sizable spontaneous AHE despite a vanishingly small net magnetization [15].

In this work we investigate the anisotropy of AHE in epitaxial Mn_5Si_3 in terms of the external field orientation relative to the crystal structure. We show that a systematic rotation of the field in different crystal planes inflicts systematic changes on the magnetotransport properties, indicating that we are able to control the relative \mathbf{L} -orientation with experimentally reasonable external field strengths of the order of 2 T. Moreover, we show that changing the relative \mathbf{L} -orientation yields anisotropic behavior of the AHE, beyond $\cos\theta$, that requires a high crystal quality of the epitaxial films and is unlikely related to the magnetocrystalline anisotropy, which further demonstrates that the properties of epitaxial Mn_5Si_3 closely match those of altermagnetic materials.

II. METHODS

The epitaxial thin films of Mn_5Si_3 are grown on Si(111) substrates by molecular beam epitaxy using optimized growth parameters for realizing films with high crystalline quality and maximum Mn_5Si_3 content [16]. A few nm-thick MnSi phase acts as a thin seed layer aiding the nucleation of Mn_5Si_3 on Si(111) [16]. Unless otherwise specified, the films used in this work contain 96 % Mn_5Si_3 and 4 % MnSi and they have a thickness of ~ 17 nm. The high crystallinity and the crystal orientation of the films have been verified using transmission electron microscopy (TEM) in our previous works [15, 16]. The epitaxial relationship between the Si substrate, MnSi seed layer and Mn_5Si_3 film is $\text{Si}(111)[1\bar{1}0]//\text{MnSi}(111)[\bar{2}11]//\text{Mn}_5\text{Si}_3(0001)[01\bar{1}0]$. The films were patterned into microscopic Hall bars shown in Figure 1(b) using optical UV lithography and subsequent ion beam etching. The orientations of the Hall bar current channels relative to the crystal axis $[2\bar{1}\bar{1}0]$ are defined by the angle α as illustrated in Figure 1(d). We measure simultaneously the longitudinal (V_{xx}) and transversal (V_{xy}) voltages (denoted in Figure 1(b,c)) as a function of the external field strength and orientation to obtain the corresponding field- and angular-dependences of the longitudinal (ρ_{xx}) and transversal (ρ_{xy}) resistivities. We apply the external field always in the (yz) plane, i.e. the plane perpendicular to the current channel. Its exact orientation relative to the $[0001]$ crystal axis (film normal) is given by the angle θ , as illustrated in Figure 1(c). Note that we will demonstrate later on in the text that the important parameter causing the anisotropic AHE is the crystal plane in which the external field rotates rather than the exact crystal orientation of the current channel - we alter the Hall bar orientation simply to ensure that the external field and the current channel are always perpendicular to each other unless otherwise stated. The current density is 3×10^5 A cm^{-2} throughout this work. For all the measurements presented in this work, the temperature was kept at 110 K, which is between the two critical temperatures of our films [15, 16]. At this temperature the films exhibit characteristic features of an altermagnetic phase, i.e. a sizable spontaneous AHE despite a vanishingly small net magnetization [15].

III. RESULTS AND DISCUSSIONS

First, we study how the AHE resistivity (ρ_{AHE}) evolves when the external field orientation, parameterized by θ , is changed. We consider a Hall bar where the external field rotates in the $(0\bar{1}10)$ plane ($\alpha = 90$ deg). We have first measured the hysteresis loops of ρ_{xy} for selected θ , from which a linear ρ_{OHE} background (slope ~ 0.045 $\mu\Omega$ cm T^{-1}), originating from the ordinary Hall effect has been removed and only the antisymmetric-in-field part of the signal is used: $\rho_{AHE} = \rho_{xy,asym} = (\rho_{xy}(H) - \rho_{xy}(-H))/2$. The symmetric part $\rho_{xy,sym} = (\rho_{xy}(H) + \rho_{xy}(-H))/2$, is negligible in our sample at the specific measurement temperature supporting the collinear spin configuration [17]. The different contributions to ρ_{xy} are summarized in Figure 2(a). For the remain-

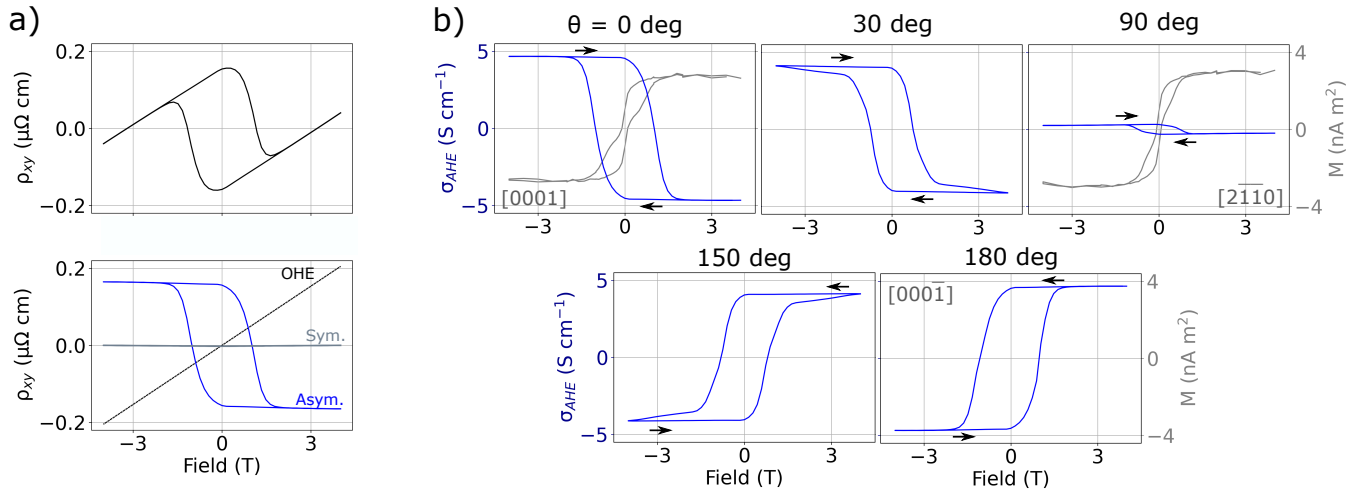


FIG. 2. (Color Online) (a) Disentangling the different contributions - symmetric-in-field $\rho_{xy,sym}$, antisymmetric-in-field $\rho_{xy,asym}$, and ordinary Hall effect ρ_{OHE} - to the field-dependence of transverse resistivity ρ_{xy} . The signal of interest here is the antisymmetric contribution, relating to the anomalous Hall effect (AHE) resistivity ρ_{AHE} . (b) The hysteresis loops of the corresponding AHE conductivity $\sigma_{AHE} = \rho_{AHE}/\rho_{xx}^2$ at selected external field orientations θ at 110 K. The sweep direction is indicated by the small arrows. The σ_{AHE} is at maximum at $\theta = 0$ deg (field out-of-plane) and decreases when the field rotates away from it, almost vanishing at $\theta = 90$ deg (field in-plane). This is in contrast with the weak magnetization M , which is isotropic for $\theta = 0$ and 90 deg. Note that we have removed the linear diamagnetic background in the hysteresis loops of M .

ing of the paper, we will convert ρ_{AHE} to AHE conductivity $\sigma_{AHE} = \rho_{AHE}/\rho_{xx}^2$, which is used to characterize the intrinsic effects (ρ_{xx} at 110 K is $\sim 180 \mu\Omega \text{ cm}$).

The hysteresis loops of σ_{AHE} for various θ are shown in Figure 2(b). We observe that the σ_{AHE} at saturation ($\sigma_{AHE,max}$) is maximum when the field is close to the out-of-plane $[0001]$ axis ($\theta = 0$ deg) and vanishes when the field is close to the in-plane $[2\bar{1}\bar{1}0]$ axis ($\theta = 90$ deg). As expected from the previous AHE study on the epitaxial Mn_5Si_3 [15], 180 degree rotation of this field changes the polarity of σ_{AHE} . The evolution of σ_{AHE} for the field orientations between $[0001]$ and $[000\bar{1}]$ is better visible in Figure 3 where we directly show σ_{AHE} as a function of θ for a 4 T external field. Between $[0001]$ and $[000\bar{1}]$ σ_{AHE} shows step-like behavior: when the field is oriented close to either $[0001]$ or $[2\bar{1}\bar{1}0]$ (in-plane) crystal axes the slope is considerably more flat than in-between these directions. We note that the backward sweep does not trace the forward sweep because the saturation is not reached at 4 T at all field orientations as seen in Figure 2(b).

To unravel the possible origin of this anisotropic behavior of the AHE, we will first study the option of weak magnetization giving a contribution. Analogously to the AHE experiments, we have measured the sample magnetization M along the external field for two field orientations $\theta = 0$ and 90 deg as shown in Figures 2b and 3. After removing a linear diamagnetic background, we observe that the magnetization loops contain two components: a non-hysteretic part that relates to the substrate and the sample holder, and a hysteretic part that we attribute to the Mn_5Si_3 film as the magnitude of its coercivity agrees with that of the AHE-signal. This hysteretic component suggests a slight spontaneous canting of the magnetic sublattice moments and can play a role in the

reversal mechanism of the Néel vector. We observe that the weak magnetization of the hysteretic component is small, i.e. $\sim 0.1 \mu_B/\text{u.c.}$, and this value for $\theta = 0$ and 90 deg is similar.

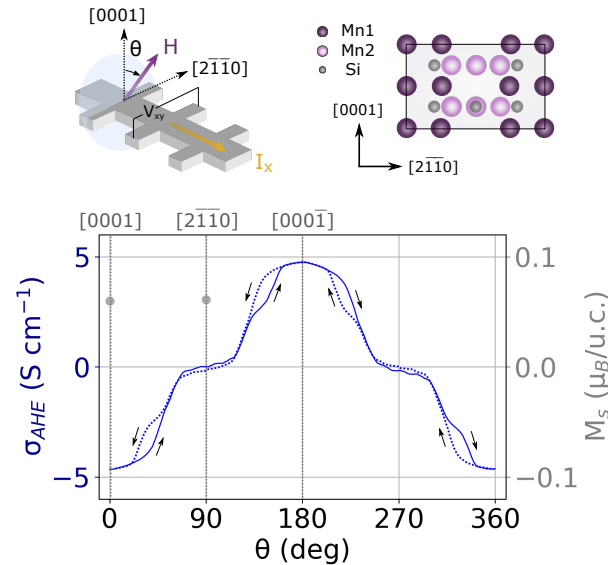


FIG. 3. (Color Online) The AHE conductivity σ_{AHE} as a function of the orientation θ of a 4 T external field, at 110 K (full line), for a current applied along the $[01\bar{1}0]$ direction ($\alpha = 90$ deg). The forward sweep is indicated by the full line and the backward sweep by the dotted line. The AHE signal does not correlate with the θ -dependence of the weak saturation magnetization M_s of the hysteretic component (circles), which is isotropic at $\theta = 0$ and 90 deg. Inset: measurement geometry recalled and crystal structure of the $(01\bar{1}0)$ plane in which the external field H is rotated.

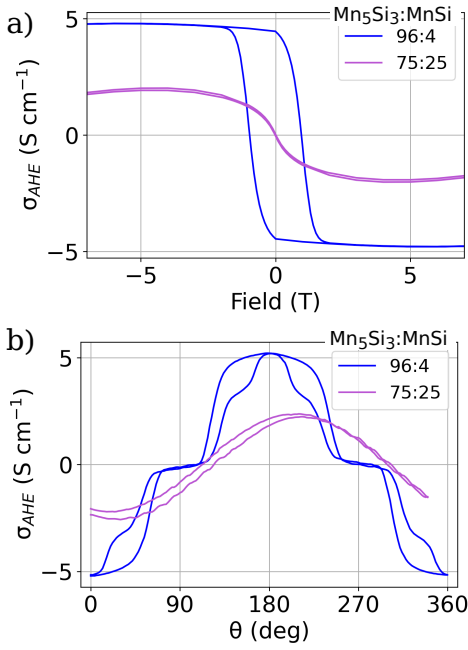


FIG. 4. (Color Online) The field strength (a) and θ -orientation (b) dependence (at 2 T) of σ_{AHE} at 110 K for epitaxial films containing 96:4 and 75:25 ratios of $Mn_5Si_3:MnSi$. The former is an altermagnetic candidate and shows sizable AHE with large coercivity and unconventional step-like θ -dependence. The latter is expected not altermagnetic and it shows smaller AHE with vanishing coercivity and conventional isotropic θ -dependence.

We note that the behavior shown in Figure 2(b) would also be expected for a ferromagnet as $M_z \sim 0$ at $\theta = 90$ deg, while the wide plateau in Figure 3 could be a consequence of the magnetocrystalline anisotropy. We will now discuss further experiments to show that the anisotropic AHE is more likely to originate from the altermagnetic phase of our films.

First, we have measured the AHE in Mn_5Si_3 films with a larger proportion of MnSi, namely 75 % Mn_5Si_3 and 25 % MnSi. Increasing the MnSi content deteriorates the crystallinity of the Mn_5Si_3 [16], leading to a more textured film. We expect this to either prohibit altermagnetism as the strain necessary for stabilizing the hexagonal unit cell can relax at the grain boundaries, or even if the hexagonal unit cell is retained in the individual grains their different crystal orientations result in overall cancelling out of the altermagnetic effects. Figure 4 confirms that the magnetotransport properties of this film are different from those of the 96:4 $Mn_5Si_3:MnSi$ Mn_5Si_3 epitaxial films with higher crystal quality. The field dependence of σ_{AHE} of the 75:25 control sample has a reduced amplitude and a vanishing coercivity, while the θ -dependence of the σ_{AHE} shows roughly a $\cos\theta$ behavior, pointing to a ferromagnetic character. These results are in stark contrast with the behavior of the 96:4 sample and demonstrate that the AHE with anisotropic θ -dependence and non-zero coercivity requires a high crystal quality of the Mn_5Si_3 epitaxial films, which is consistent with the altermagnetic phase being at the origin of the AHE requiring the system to have a specific symmetry. Moreover, this shows that the spurious MnSi phase

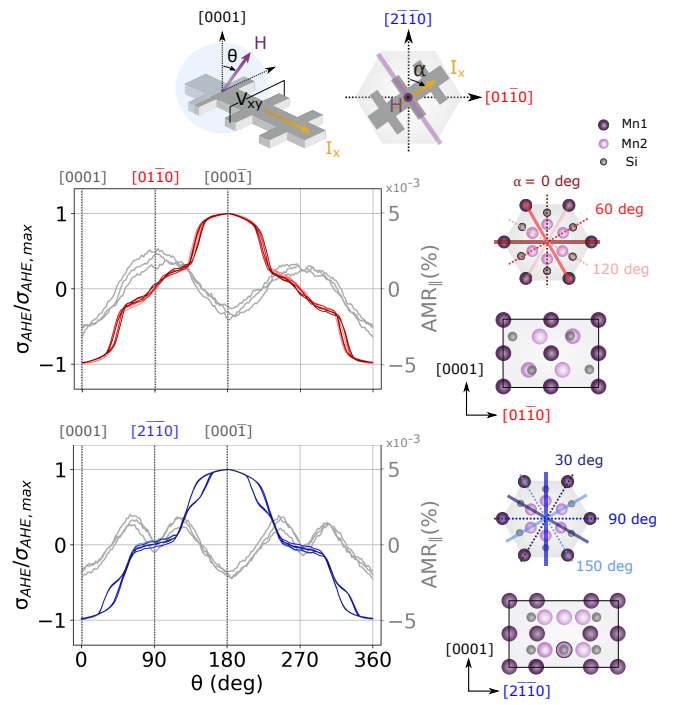


FIG. 5. (Color Online) The normalized AHE conductivity $\sigma_{AHE}/\sigma_{AHE,max}$ and the longitudinal anisotropic magnetoresistance ($AMR_{||}$) when the external field is rotated in different crystal planes. In both cases, two distinct behaviors can be observed depending on whether the crystal plane is equivalent to $(0\bar{1}10)$ or $(2\bar{1}\bar{1}0)$. Here, the field strength is 4 T and the temperature is 110 K. The inserts recall the geometry used and the planes in which the field is rotated.

with $T_c \sim 40$ K is also unlikely origin of the AHE signal as the σ_{AHE} should in that case be stronger for the 75:25 sample.

Next, to further study the anisotropy of AHE, we vary systematically the crystal plane in which the external field and in effect the Néel vector \mathbf{L} (confirmed later using the anisotropic magnetoresistance measurements) is rotated and again observe how the σ_{AHE} is affected. This was realized by patterning multiple Hall bars with their current channels oriented along different crystal axes. We recall that these orientations are denoted by α , which is the angle between the current channel and the crystal axis $[2\bar{1}\bar{1}0]$ as was shown in Figure 1(d). For each Hall bar we rotate the field in a plane perpendicular to the current channel and thus effectively we are changing the crystal plane in which the field rotates. We have selected α 's that reflect the hexagonal crystal structure of our material and can be divided into two sets: for $\alpha = 0, 60, 120$ deg the current channel is along $[2\bar{1}\bar{1}0]$ or equivalent so the field rotates in the crystal plane $(2\bar{1}\bar{1}0)$ or equivalent; for $\alpha = 30, 90, 150$ deg the current channel is along $[0\bar{1}10]$ or equivalent and the field rotates in the crystal plane $(0\bar{1}10)$ or equivalent. In Figure 5 we show the θ -dependence of the σ_{AHE} (with 4 T field) for the two sets of α 's. For each set, σ_{AHE} is maximum when the field is close to $[0001]$ axis but significant differences arise when the field orients towards the sample plane: for $\alpha = 30, 90, 150$

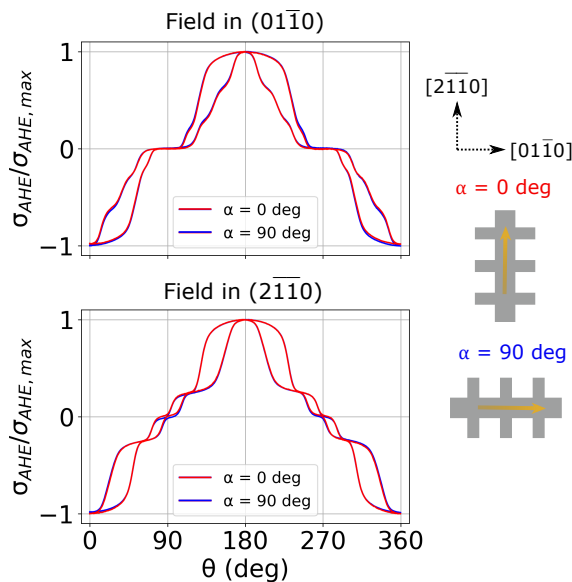


FIG. 6. (Color Online) Two perpendicular Hall bars measured simultaneously at 110 K with 2 T field. The anisotropic θ -dependence of σ_{AHE} relates to the crystal plane in which the field rotates instead of the crystal axis along which the current channel orients.

deg, when the field orients in the $[2\bar{1}\bar{1}0]$ direction or equivalent, we observe a wide plateau around $\theta = 90$ deg, familiar from Figure 3, while for $\alpha = 0, 60, 120$ deg when the field orients in the $[0\bar{1}10]$ direction or equivalent we observe a steeper linear slope instead. We have verified that this anisotropy persists also at 2 and 7 T fields. The hexagonal symmetry of the AHE signals for the different α suggests that the three possibilities for the distribution of the magnetic Mn2 atoms (Figure 1) are likely present in equal populations: if each Mn2 site is on average magnetic, the α -dependence of σ_{AHE} should reflect the hexagonal symmetry of the crystal structure. If one of these 'quadrupole domains' dominated, lower symmetry for the α -dependence of σ_{AHE} would be expected. We have verified that the key factor responsible for the change of behavior between the different α s is the crystal plane in which the field rotates rather than the crystal axis along which the current channel is oriented, as observed in Figure 6. We note that for Figure 6 we have used a different sample of the same material, which explains some of the differences in the θ -dependence of the σ_{AHE} compared to the other figures. However, the overall behavior is the same, which confirms the reproducibility of the results discussed here. In summary, the results in Figures 5 and 6 allow us to conclude that the anisotropic behavior depends on the \mathbf{L} -orientation relative to the hexagonal crystal symmetry of the Mn_5Si_3 epitaxial films.

We also consider magnetocrystalline anisotropy as the origin of the anisotropic AHE unlikely: if we interpret the results shown in Figures 3 and 5 considering that the different crystal planes have strongly different magnetocrystalline energy landscapes, then for $\alpha = 30, 90,$ and 150 deg it is more energetically favorable for \mathbf{L} to remain aligned along a crystal axis yielding $\sigma_{AHE} = 0$ at $\theta = 90$ deg compared to $\alpha = 0, 60,$ and

120 deg. However, the hysteresis loops measured at $\theta = 90$ deg for both $\alpha = 0$ (not shown) and 90 deg (Figure 2(b)) superimpose at 4 T, indicating that it is unlikely that at this field \mathbf{L} is lagging behind the external field around $\theta = 90$ deg for $\alpha = 30, 90,$ and 150 deg more than for $\alpha = 0, 60,$ and 120 deg. Moreover, we observe the anisotropy in the α -dependence of σ_{AHE} persisting up to 7 T, which is well above the saturation field of σ_{AHE} at any θ , as shown in Figure 2(b). Along with our demonstration that the anisotropic AHE is crystal quality-dependent and depends on the \mathbf{L} -orientation relative to the hexagonal crystal symmetry, these observations provide further support to the main AHE contribution in our Mn_5Si_3 films being from altermagnetism. These results constitute the main conclusion of our work and they systematically support the previous calculations and experiments on the same system [15].

Finally, we confirm the ability to manipulate \mathbf{L} with the external field by measuring the anisotropic magnetoresistance (AMR), which is known to depend on the \mathbf{L} -orientation. As shown in Figure 5, we have measured the α - and θ -dependence of the longitudinal AMR ($\text{AMR}_{||}$), which relates to ρ_{xx} as $\text{AMR}_{||}(\theta) = (\rho_{xx}(\theta) - \langle \rho_{xx} \rangle) / \langle \rho_{xx} \rangle$, where $\langle \rho_{xx} \rangle$ indicates ρ_{xx} averaged over all angles. AMR is an even function of the field and known to have two components: a non-crystalline one scaling with the angle between the order parameter and the current directions, and a crystalline one relating to the order parameter orientation relative to the crystal axes [36]. We show the θ -dependence for $\alpha = 0, 60, 120$ deg and $\alpha = 30, 90, 150$ deg Hall bars in Figure 5 at conditions identical to the AHE measurements. Again we observe different behaviors for the two sets of α , as expected from the crystalline AMR depending on the crystal plane in which the order parameter rotates: for $\alpha = 0, 60, 120$ deg the dependence follows a $\cos 2\theta$ behavior while for $\alpha = 30, 90, 150$ deg higher order even cosines appear in the signal.

Although the exact Néel vector orientation and rotation under the action of the external magnetic field cannot be deduced from the results presented, in this final paragraph we wish to open a discussion on the interpretation of the anisotropic AHE in the light of the symmetries of the epitaxial Mn_5Si_3 considering this material to be a strong candidate for the altermagnetic phase. First, it should be noted that in our measurement geometry (Figure 1), the changes in σ_{AHE} correspond to changes in the component of \mathbf{h} along the $[0001]$ direction (out-of-plane). In altermagnets, the presence and orientation of \mathbf{h} depend on the \mathbf{L} -vector orientation because the latter influences the symmetries of the system. While accurate calculation of the entire θ -dependence of $\mathbf{h}(\mathbf{L})$ is inhibited by the unknown relevant micromagnetic parameters, the value of σ_{AHE} for some specific orientations can be inferred from symmetry-considerations. The symmetry analysis on the expected spin structure of the epitaxial Mn_5Si_3 shown in Figure 1(a) indicates that for non-zero σ_{AHE} the \mathbf{L} -vector cannot point along the $[0001]$ axis (\mathbf{h} excluded), along the main in-plane axes (only \mathbf{h} in-plane allowed), or in the planes of the high-symmetry in-plane axes highlighted in Figure 1(a) (only \mathbf{h} in-plane allowed). Here, the crystal symmetries of the planes corresponding to $\alpha = 0, 60,$ and 120 deg and $\alpha = 30,$

90, and 150 deg differ, as seen in Figure 5 and therefore the σ_{AHE} likely differ, too.

IV. CONCLUSION

In conclusion, the implications of our measurements on the external field orientation dependence of σ_{AHE} in epitaxial Mn_5Si_3 films are two-fold. First, the systematic changes in σ_{AHE} supported by the systematic changes in AMR_{\parallel} upon the field rotation underlines our ability to manipulate the \mathbf{L} -orientation with an external field of the order of 2 T or more. This is an important premise for further experimentally feasible spin transport studies in altermagnets where control over the \mathbf{L} -orientation is critical. Second, our key result is that the σ_{AHE} in epitaxial Mn_5Si_3 films shows anisotropic behavior as a function of the external field-induced orientation of \mathbf{L} rel-

ative to the underlying crystal structure, and this anisotropic behavior depends on the crystal quality and is unlikely to relate to the magnetocrystalline anisotropy. This observation of the anisotropic σ_{AHE} adds to the growing array of properties of epitaxial Mn_5Si_3 advocating the altermagnetic phase in this material.

ACKNOWLEDGMENTS

This work was supported by the French national research agency (ANR) and the Deutsche Forschungsgemeinschaft (DFG) (Project MATHEEIAS- Grant No. ANR-20-CE92-0049-01 / DFG-445976410). H. R., E. S., S. T. B. G. and A. T. are supported by the DFG-GACR grant no. 490730630. J. R. acknowledges MINECO for the Margaritas Salas program. D. K. acknowledges the academy of sciences of the Czech Republic for the Lumina quaeruntur program.

-
- [1] N. Nagaosa, J. Sinova, S. Onoda, A. H. MacDonald, and N. P. Ong, Anomalous Hall effect, *Rev. Mod. Phys.* **82**, 1539 (2010).
- [2] J. Kübler and C. Felser, Non-collinear antiferromagnets and the anomalous Hall effect, *EPL (Europhysics Letters)* **108**, 67001 (2014).
- [3] H. Chen, Q. Niu, and A. H. MacDonald, Anomalous Hall effect arising from noncollinear antiferromagnetism, *Phys. Rev. Lett.* **112**, 017205 (2014).
- [4] S. Nakatsuji, N. Kiyohara, and T. Higo, Large anomalous Hall effect in a non-collinear antiferromagnet at room temperature, *Nature* **527**, 212 (2015).
- [5] A. K. Nayak, J. E. Fischer, Y. Sun, B. Yan, J. Karel, A. C. Komarek, C. Shekhar, N. Kumar, W. Schnelle, J. Kübler, C. Felser, and S. S. P. Parkin, Large anomalous Hall effect driven by a nonvanishing Berry curvature in the noncollinear antiferromagnet M_3Ge , *Science Advances* **2**, e1501870 (2016).
- [6] L. Šmejkal, R. González-Hernández, T. Jungwirth, and J. Sinova, Crystal time-reversal symmetry breaking and spontaneous Hall effect in collinear antiferromagnets, *Science Advances* **6**, eaaz8809 (2020).
- [7] L. Šmejkal, A. H. MacDonald, J. Sinova, S. Nakatsuji, and T. Jungwirth, Anomalous Hall antiferromagnets, *Nature Reviews Materials* **7**, 482 (2022).
- [8] T. Jungwirth, X. Marti, P. Wadley, and J. Wunderlich, Antiferromagnetic spintronics, *Nature Nanotechnology* **11**, 231–241 (2016).
- [9] V. Baltz, A. Manchon, M. Tsoi, T. Moriyama, T. Ono, and Y. Tserkovnyak, Antiferromagnetic spintronics, *Rev. Mod. Phys.* **90**, 015005 (2018).
- [10] L. Šmejkal, J. Sinova, and T. Jungwirth, Beyond conventional ferromagnetism and antiferromagnetism: A phase with nonrelativistic spin and crystal rotation symmetry, *Phys. Rev. X* **12**, 031042 (2022).
- [11] Z. Feng, X. Zhou, L. Šmejkal, L. Wu, Z. Zhu, H. Guo, R. González-Hernández, X. Wang, H. Yan, P. Qin, X. Zhang, H. Wu, H. Chen, Z. Meng, L. Liu, Z. Xia, J. Sinova, T. Jungwirth, and Z. Liu, An anomalous Hall effect in altermagnetic ruthenium dioxide, *Nature Electronics* **5**, 735 (2022).
- [12] T. Tschirner, P. Keßler, R. D. Gonzalez Betancourt, T. Kotte, D. Kriegner, B. Büchner, J. Dufouleur, M. Kamp, V. Jovic, L. Smejkal, J. Sinova, R. Claessen, T. Jungwirth, S. Moser, H. Reichlova, and L. Veyrat, Saturation of the anomalous hall effect at high magnetic fields in altermagnetic ruO_2 , *APL Materials* **11**, 10.1063/5.0160335 (2023).
- [13] R. D. Gonzalez Betancourt, J. Zubáč, R. Gonzalez-Hernandez, K. Geishendorf, Z. Šobáň, G. Springholz, K. Olejník, L. Šmejkal, J. Sinova, T. Jungwirth, S. T. B. Goennenwein, A. Thomas, H. Reichlová, J. Železný, and D. Kriegner, Spontaneous anomalous Hall effect arising from an unconventional compensated magnetic phase in a semiconductor, *Phys. Rev. Lett.* **130**, 036702 (2023).
- [14] K. P. Kluczyk, K. Gas, M. J. Grzybowski, P. Skupiński, M. A. Borysiewicz, T. Fas, J. Suffczyński, J. Z. Domagala, K. Graszka, A. Mycielski, M. Baj, K. H. Ahn, K. Výborný, M. Sawicki, and M. Gryglas-Borysiewicz, Coexistence of anomalous Hall effect and weak net magnetization in collinear antiferromagnet $MnTe$ (2023), [arXiv:2310.09134](https://arxiv.org/abs/2310.09134).
- [15] H. Reichlová, R. L. Seeger, R. González-Hernández, I. Kounta, R. Schlitz, D. Kriegner, P. Ritzinger, M. Lammel, M. Leiviskä, V. Petříček, P. Doležal, E. Schmoranzzerová, A. Bad'ura, A. Thomas, V. Baltz, L. Michez, J. Sinova, S. T. B. Goennenwein, T. Jungwirth, and L. Šmejkal, Macroscopic time reversal symmetry breaking by staggered spin-momentum interaction (2021), [arXiv:2012.15651](https://arxiv.org/abs/2012.15651) [*cond-mat.mes-hall*].
- [16] I. Kounta, H. Reichlova, D. Kriegner, R. Lopes Seeger, A. Bad'ura, M. Leiviska, A. Boussadi, V. Heresanu, S. Bertaina, M. Petit, E. Schmoranzzerova, L. Smejkal, J. Sinova, T. Jungwirth, V. Baltz, S. T. B. Goennenwein, and L. Michez, Competitive actions of $MnSi$ in the epitaxial growth of Mn_5Si_3 thin films on $Si(111)$, *Phys. Rev. Mater.* **7**, 024416 (2023).
- [17] A. Badura, D. Kriegner, E. Schmoranzzerová, K. Výborný, M. Leiviskä, R. L. Seeger, V. Baltz, D. Scheffler, S. Beckert, I. Kounta, L. Michez, L. Šmejkal, J. Sinova, S. T. B. Goennenwein, J. Železný, and H. Reichlová, Even-in-magnetic-field part of transverse resistivity as a probe of magnetic order (2023), [arXiv:2311.14498](https://arxiv.org/abs/2311.14498).

- [18] O. Fedchenko, J. Minar, A. Akashdeep, S. W. D'Souza, D. Vasilyev, O. Tkach, L. Odenbreit, Q. L. Nguyen, D. Kutnyakhov, N. Wind, L. Wenthous, M. Scholz, K. Rossnagel, M. Hoesch, M. Aeschlimann, B. Stadtmueller, M. Kläui, G. Schoenhense, G. Jakob, T. Jungwirth, L. Smejkal, J. Sinova, and H. J. Elmers, Observation of time-reversal symmetry breaking in the band structure of altermagnetic RuO₂ (2023), [arXiv:2306.02170](#).
- [19] S. Lee, S. Lee, S. Jung, J. Jung, D. Kim, Y. Lee, B. Seok, J. Kim, B. G. Park, L. Smejkal, C.-J. Kang, and C. Kim, Broken Kramers' degeneracy in altermagnetic MnTe (2023), [arXiv:2308.11180](#).
- [20] T. Osumi, S. Souma, T. Aoyama, K. Yamauchi, A. Honma, K. Nakayama, T. Takahashi, K. Ohgushi, and T. Sato, Observation of giant band splitting in altermagnetic MnTe (2023), [arXiv:2308.10117](#).
- [21] S. Reimers, L. Odenbreit, L. Smejkal, V. N. Strocov, P. Constantinou, A. B. Hellenes, R. J. Ubierno, W. H. Campos, V. K. Bharadwaj, A. Chakraborty, T. Denneulin, W. Shi, R. E. Dunin-Borkowski, S. Das, M. Kläui, J. Sinova, and M. Jourdan, Direct observation of altermagnetic band splitting in CrSb thin films (2023), [arXiv:2310.17280](#).
- [22] R. M. Sattigeri, G. Cuono, and C. Autieri, Altermagnetic surface states: towards the observation and utilization of altermagnetism in thin films, interfaces and topological materials, *Nanoscale* **15**, 16998–17005 (2023).
- [23] X. Zhou, W. Feng, R.-W. Zhang, L. Smejkal, J. Sinova, Y. Mokrousov, and Y. Yao, Crystal thermal transport in altermagnetic RuO₂ (2023), [arXiv:2305.01410](#).
- [24] R. González-Hernández, L. Smejkal, K. Výborný, Y. Yahagi, J. Sinova, T. c. v. Jungwirth, and J. Železný, Efficient electrical spin splitter based on nonrelativistic collinear antiferromagnetism, *Phys. Rev. Lett.* **126**, 127701 (2021).
- [25] A. Bose, N. J. Schreiber, R. Jain, D.-F. Shao, H. P. Nair, J. Sun, X. S. Zhang, D. A. Muller, E. Y. Tsybal, D. G. Schlom, and D. C. Ralph, Tilted spin current generated by the collinear antiferromagnet ruthenium dioxide, *Nature Electronics* **5**, 267–274 (2022).
- [26] H. Bai, L. Han, X. Y. Feng, Y. J. Zhou, R. X. Su, Q. Wang, L. Y. Liao, W. X. Zhu, X. Z. Chen, F. Pan, X. L. Fan, and C. Song, Observation of spin splitting torque in a collinear antiferromagnetic RuO₂, *Phys. Rev. Lett.* **128**, 197202 (2022).
- [27] B. Chi, L. Jiang, Y. Zhu, G. Yu, C. Wan, J. Zhang, and X. Han, Crystal facet orientated altermagnets for detecting ferromagnetic and antiferromagnetic states by giant tunneling magnetoresistance effect (2023), [arXiv:2309.09561](#).
- [28] L. Smejkal, A. B. Hellenes, R. González-Hernández, J. Sinova, and T. Jungwirth, Giant and Tunneling magnetoresistance in unconventional collinear antiferromagnets with nonrelativistic spin-momentum coupling, *Phys. Rev. X* **12**, 011028 (2022).
- [29] S. Xu, Z. Zhang, F. Mahfouzi, Y. Huang, H. Cheng, B. Dai, W. Cai, K. Shi, D. Zhu, Z. Guo, C. Cao, Y. Liu, A. Fert, N. Kioussis, K. L. Wang, Y. Zhang., and W. Zhao, Spin-flop magnetoresistance in a collinear antiferromagnetic tunnel junction (2023), [arXiv:2311.02458](#).
- [30] W. Limmer, M. Glunk, J. Daeubler, T. Hummel, W. Schoch, R. Sauer, C. Bihler, H. Huebl, M. S. Brandt, and S. T. B. Goennenwein, Angle-dependent magnetotransport in cubic and tetragonal ferromagnets: Application to (001)- and (113) α -oriented (Ga,Mn)As, *Phys. Rev. B* **74**, 205205 (2006).
- [31] E. Roman, Y. Mokrousov, and I. Souza, Orientation dependence of the intrinsic anomalous Hall effect in hcp cobalt, *Phys. Rev. Lett.* **103**, 097203 (2009).
- [32] G. H. Lander, P. J. Brown, and J. B. Forsyth, The antiferromagnetic structure of Mn₅Si₃, *Proceedings of the Physical Society* **91**, 332 (1967).
- [33] A. Z. Menshikov, A. P. Vokhmyanin, and Y. A. Dorofeev, Magnetic structure and phase transformations in Mn₅Si₃, *physica status solidi (b)* **158**, 319 (1990).
- [34] P. J. Brown, J. B. Forsyth, V. Nunez, and F. Tasset, The low-temperature antiferromagnetic structure of Mn₅Si₃ revised in the light of neutron polarimetry, *Journal of Physics: Condensed Matter* **4**, 10025 (1992).
- [35] P. J. Brown and J. B. Forsyth, Antiferromagnetism in Mn₅Si₃: the magnetic structure of the AF2 phase at 70 K, *Journal of Physics: Condensed Matter* **7**, 7619 (1995).
- [36] A. W. Rushforth, K. Výborný, C. S. King, K. W. Edmonds, R. P. Champion, C. T. Foxon, J. Wunderlich, A. C. Irvine, P. Vašek, V. Novák, K. Olejník, J. Sinova, T. Jungwirth, and B. L. Gallagher, Anisotropic magnetoresistance components in (Ga,Mn)As, *Phys. Rev. Lett.* **99**, 147207 (2007).